JGR Oceans

RESEARCH ARTICLE
10.1029/2020JC016893

Wintertime Water Mass Transformation in the Western Iceland and Greenland Seas

Jie Huang[1,2], Robert S. Pickart[2], Frank Bahr[2], Leah T. McRaven[2], and Fanghua Xu[1,3]

[1]Department of Earth System Science, Ministry of Education Key Laboratory for Earth System Modeling, Tsinghua University, Beijing, China, [2]Woods Hole Oceanographic Institution, Woods Hole, MA, USA, [3]Southern Marine Science and Engineering Guangdong Laboratory, Zhuhai, China

Key Points:

- A wintertime survey of the western Iceland and Greenland Seas was conducted in February-March 2018
- Atlantic- and Arctic-origin Overflow Water was ventilated at the offshore edge of East Greenland Current and in the interior, respectively
- Cold-air outbreaks and eddies play important roles in modifying the ventilation of overflow water in the western Iceland and Greenland Seas

Correspondence to:
J. Huang,
j1eson2017@gmail.com

Citation:
Huang, J., Pickart, R. S., Bahr, F., McRaven, L. T., & Xu, F. (2021). Wintertime water mass transformation in the western Iceland and Greenland Seas. *Journal of Geophysical Research: Oceans*, *126*, e2020JC016893. https://doi.org/10.1029/2020JC016893

Received 21 OCT 2020
Accepted 10 JUL 2021

Abstract Hydrographic and velocity data from a 2018 winter survey of the western Iceland and Greenland Seas are used to investigate the ventilation of overflow water feeding Denmark Strait. We focus on the two general classes of overflow water: warm, saline Atlantic-origin Overflow Water (AtOW) and cold, fresh Arctic-origin Overflow Water (ArOW). The former is found predominantly within the East Greenland Current (EGC), while the latter resides in the interior of the Iceland and Greenland Seas. Progressing north to south, the properties of AtOW in the EGC are modified diapycnally during the winter, in contrast to summer when along-isopycnal mixing dominates. The water column response to a 10-days cold-air outbreak was documented using repeat observations. During the event, the northerly winds pushed the freshwater cap of the EGC onshore, and convection modified the water at the seaward edge of the current. Lateral transfer of heat and salt from the core of AtOW in the EGC appears to have influenced some of this water mass transformation. The long-term evolution of the mixed layers in the interior was investigated using a 1-D mixing model. This suggests that, under strong atmospheric forcing, the densest component of ArOW can be ventilated in this region. Numerous anti-cyclonic eddies spawned from the EGC were observed during the winter survey, revealing that these features can play differing roles in modifying/prohibiting the open-ocean convection.

Plain Language Summary A rare wintertime shipboard survey of the western Iceland and Greenland Seas was conducted in February-March 2018. The goal was to better understand the formation of dense water that flows southward through Denmark Strait, between Greenland and Iceland. This water contributes to circulation of the North Atlantic, which affects Earth's climate. Two types of dense water masses were investigated, one found predominantly in the East Greenland Current flowing southward along the continental slope, and the other in the interior of the Iceland and Greenland Seas. The dense water in the boundary is modified by air-sea heat exchange, in contrast to summer when it is altered by ocean mixing. The response to a 10-days cold-air outbreak was documented, revealing how the wind, air-sea heat flux, and ocean mixing can contribute to the modification of the water at the seaward edge of the boundary current. Using a simple model, we demonstrated that—under sustained strong atmospheric forcing—the interior water becomes very dense. Finally, small swirls of water emanating from the boundary current can strongly modify the air-sea interaction in the interior. Our results shed light on a critical process at high latitudes that impacts Earth's climate system.

1. Introduction

The Nordic Seas (collectively the Norwegian, Greenland and Iceland Seas) play a critical role in the North Atlantic climate system. It is where warm and saline subtropical-origin water is transformed into cold and dense overflow water (Chafik & Rossby, 2019; Dickson & Brown, 1994; Mauritzen, 1996). The dense water (potential density $\sigma_\theta \geq 27.8$ kg/m^3) sinks and returns southward, comprising the deepest limb of the Atlantic Meridional Overturning Circulation (AMOC) (Eldevik et al., 2009; Hansen & Østerhus, 2000; Olsen et al., 2008). There are two general classes of overflow water in the Nordic Seas: Atlantic-origin Overflow Water, AtOW ($\sigma_\theta \geq 27.8$ kg/m^3 and potential temperature $\theta \geq 0$°C) and Arctic-origin Overflow Water, ArOW($\sigma_\theta \geq 27.8$ kg/m^3 and $\theta < 0$°C) (Hansen & Østerhus, 2000; Mastropole et al., 2017; Våge et al., 2011). AtOW is formed by strong air-sea heat loss along the rim current system encircling the Nordic Seas (Mauritzen, 1996). It is transported to Denmark Strait by the East Greenland Current (EGC) (Mauritzen, 1996) (Figure 1). ArOW is produced via wintertime open-ocean convection in the interior of Greenland and

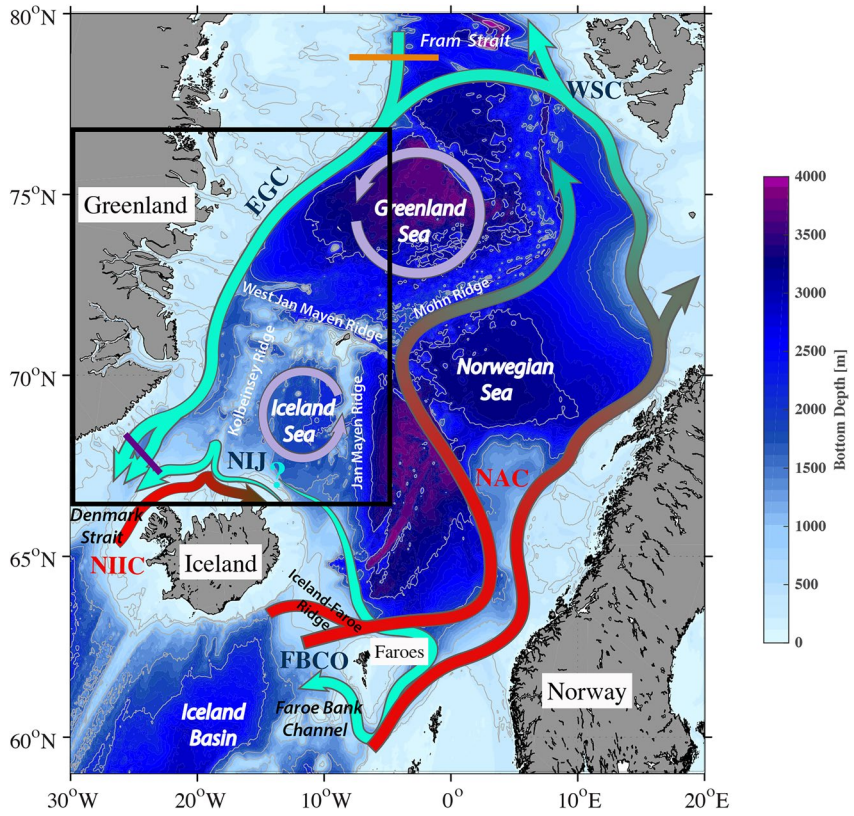

Figure 1. Schematic circulation of the Nordic Seas, modified from Huang et al. (2020). The pathways of warm Atlantic inflow, dense outflow, and cyclonic gyre circulation in the Greenland and Iceland Seas are shown by the red, green, and purple arrows, respectively. Colors and gray contours represent the bathymetry from ETOPO2, and the relevant ridges are named. The abbreviations are: NAC, Norwegian Atlantic Current; WSC, West Spitsbergen Current; NIIC, North Icelandic Irminger Current; EGC, East Greenland Current; NIJ, North Icelandic Jet; FBCO, Faroe Bank Channel overflow. The orange and purple lines indicate, respectively, the location of a mooring array deployed south of Fram Strait (de Steur et al., 2014) and a mooring array deployed north of Denmark Strait (Harden et al., 2016). The region considered in this study is outlined by the black box.

Iceland Seas (Mastropole et al., 2017; Swift et al., 1980; Våge et al., 2011, 2015). It is advected to Denmark Strait via the North Icelandic Jet (NIJ) (Semper et al., 2019; Våge et al., 2013) (Figure 1). Using historical hydrographic data and an end-member analysis, Mastropole et al. (2017) revealed that the ArOW occupies the deepest part of Denmark Strait, whereas the AtOW resides above this and to the west, in the vicinity of the East Greenland shelf break. While the circulation scheme in the Nordic Seas has been updated as a result of the discovery of the NIJ, there remain many questions regarding the sources, transformation, and variability of the overflow water.

Previous studies of the EGC, and the AtOW that it transports, have mainly focused on the regions close to Fram and Denmark Straits (de Steur et al., 2009, 2014; Fahrbach et al., 2001; Foldvik et al., 1988; Harden et al., 2016; Håvik, Våge, et al., 2017; Håvik & Våge, 2018; Lin et al., 2020). Based on a long-term (1997–2009) mooring array deployed south of Fram Strait (orange line in Figure 1), de Steur et al. (2014) found that the annual mean transport of the EGC is 8.7 Sv (1 Sv = 10^6 m^3/s) at 78.8°N (including 3 Sv transported by the recirculation of the West Spitsbergen Current). However, de Steur et al. (2014) did not estimate the transport of AtOW in the EGC. Using a year-long mooring array deployed roughly 200 km north of Denmark Strait (purple line in Figure 1), Harden et al. (2016) found that the annual transport of AtOW by the EGC is 2.54 ± 0.17 Sv. By analyzing a set of shipboard hydrographic-velocity sections along the transect at Denmark Strait, Lin et al. (2020) estimated the total mean transport of AtOW to be 1.49 ± 0.10 Sv. For the regions between the two straits, the EGC and AtOW have been only sparsely observed. Rudels et al. (2002, 2005) reported on data from two cruises (fall of 1998 and summer of 2002) that sampled the EGC from Fram Strait

to Denmark Strait. Their focus was on the hydrography, and several different water masses were defined within the current (Nilsson et al., 2008; Rudels et al., 2002, 2005). They identified warm Re-circulating Atlantic Water and cold Arctic Intermediate Water, which have similar characteristics to the AtOW and ArOW, respectively. Håvik, Pickart, et al. (2017) presented both the water mass and kinematic structure of the EGC from Fram Strait to Denmark Strait from a high-resolution shipboard survey in summer 2012. They identified two distinct velocity cores of the EGC: the well-known shelfbreak branch, and a separate branch seaward of the shelf edge. The estimated transport of AtOW water by the shelfbreak branch was 2.8 ± 0.7 Sv. While previous studies have documented the variability of the EGC near Denmark and Fram Straits (de Steur et al., 2014; Harden et al., 2016; Håvik, Våge, et al., 2017), no studies have investigated the along-stream variation in water mass and kinematic structure of the EGC in the winter season. In the past it was thought that AtOW subducted under the ice near Fram Strait, prohibiting any further densification of the water as it flowed south in the EGC (Mauritzen, 1996). However, recent glider data from the Iceland Sea has shown that wintertime re-ventilation of the AtOW can occur over the continental slope due to the decreasing ice cover (Våge et al., 2018).

The western Iceland and Greenland Seas are also important with regard to the source of ArOW. Since the NIJ was discovered to transport nearly all of the ArOW to Denmark Strait (Jonsson & Valdimarsson, 2004; Våge et al., 2011), debates have ensued as to where the NIJ originates from (Käse et al., 2009; Köhl et al., 2007; Köhl, 2010). Våge et al. (2011) hypothesized that the NIJ sources from the Iceland Sea gyre. In this scheme, the North Icelandic Irminger Current (NIIC, Figure 1) turbulently transports warm subtropical-origin water to the central Iceland Sea, where densification of the water takes place under strong air-sea interaction in winter. However, Våge et al. (2015) subsequently demonstrated that the deepest and densest late-winter mixed layers occur in the northwest Iceland Sea, suggesting that some of the water in the NIJ originates from the periphery of the Iceland Sea gyre. By analyzing the interannual variability in the salinity of the NIJ and NIIC, Pickart et al (2017) suggested that densification of ArOW occurs in different areas. The northern Iceland shelf and east of the Kolbeinsey Ridge were considered as potential source regions of the NIJ by analyzing Lagrangian trajectories of particles in a high-resolution numerical model (Behrens et al., 2017). Using RAFOS float data from the Iceland Sea, de Jong et al (2018) hypothesized a western source of the NIJ near the east Greenland slope. Most recently, Huang et al. (2020) argued that the ArOW in the NIJ stems mainly from the Greenland Sea gyre. They deduced this by invoking a new water mass metric to trace the so-called NIJ transport mode water (Semper et al., 2019) in a potential-density/potential-spicity framework. Huang et al. (2020) also suggested that the northwest Iceland Sea supplies a smaller fraction of the ArOW (consistent with the glider measurements of Våge et al., 2018); however, there are significant data gaps in this region during winter.

The atmospheric forcing in the western Iceland and Greenland Seas is complex, depending largely on the interplay between two centers of action: the Icelandic Low and Lofoten Low. While the annual mean air-sea heat flux is moderate in the region, this is due to a combination of high and low heat flux events throughout the winter (Moore et al., 2012). When the Icelandic Low is deep, corresponding to a positive phase of the the North Atlantic Oscillation (NAO), warm air from the south and east is advected over the western Iceland and Greenland Seas resulting in weak ocean cooling (or even warming) (Renfrew et al., 2019). When the NAO is in the negative phase, a deepened Lofoten Low is associated with cold-air outbreaks in the region (e.g., Jahnke-Bornemann & Brümmer, 2008). These outbreaks result in high air-sea turbulent heat fluxes ($\sim$200 W m^{-2}). While each cold-air outbreak only lasts 2–4 days, they occur every 1–2 weeks and account for the majority of the ocean heat loss in the western Iceland and Greenland Seas (Harden et al., 2015).

In an effort to further our understanding of the wintertime air-sea interaction in the western Nordic Seas, and the role this plays in the ventilation of overflow waters feeding Denmark Strait, the Iceland-Greenland Seas Project (IGP) was carried out February-March 2018 (Renfrew et al., 2019). This included a joint ship/aircraft field operation, use of numerical simulations, and analysis of historical data. In this study, we analyze the wintertime cruise data to shed light on the ventilation process. We note that in this context we are equating ventilation with outcropping of a given water mass at the surface during winter, as opposed to subduction which happens when the water mass is transferred into the interior during the late spring and summer. We begin with a broad view of the wintertime hydrographic and kinematic conditions encountered in the western Iceland and Greenland Seas. A previous summertime survey of the region is used to help

quantify the seasonality. Next, we investigate the ventilation of both AtOW and ArOW in the vicinity of the boundary current (EGC) and in the interior. In particular, we characterize the wintertime transformation of AtOW along the pathway of the EGC and its response to a cold-air outbreak. We then explore the influence of eddy activity on freshwater transport and the role this plays on water mass transformation in the interior. Finally, we investigate the source region of ArOW in the interior of western Iceland and Greenland Seas.

2. Data and Methods

2.1. Winter Cruise Data

The wintertime hydrographic and velocity data used in the study were collected on the NRV *Alliance* in winter 2018. The cruise had two legs: the first during 6–21 February, and the second from 26 February to 22 March. One of the unique aspects of the IGP was the coordinated sampling carried out between *Alliance* and the Meteorological Airborne Science Instrumentation (MASIN) aircraft (see Renfrew et al., 2019). Studies using the aircraft data, and collaborative analyses using both data sets, are ongoing. The present study focuses on the shipboard data.

A Sea-Bird 911+ conductivity-temperature-depth (CTD) instrument was attached on a frame with twelve 5-L Niskin bottles for seawater sampling. Profiles of CTD temperature and salinity were averaged into 2 dbar bins. The CTD salinity data were then calibrated using the water sample salinity data. The resulting accuracy of the CTD measurements is 0.3 dbar for pressure, 0.001°C for temperature, and 0.009 for salinity. To supplement the hydrographic data, expendable CTDs (XCTDs, with a maximum measurement depth of 1,000 m) were used, particularly in inclement weather. In order to assess the accuracy of the XCTD measurements, some of the expendables were dropped simultaneously with CTD casts. XCTD salinity profiles were calculated using the Gibbs Seawater Oceanographic toolbox, then the temperature and salinity profiles were averaged into 2-m bins. These were compared in density-space to the corresponding CTD profiles. After iteratively removing outliers greater than three standard deviations, temperature and salinity differences of -0.03 ± 0.01°C and -0.01 ± 0.001 (mean ± standard error) were found between XCTD and CTD measurements. A linear fit ($R > 0.97$) was applied to all of the XCTD profiles to adjust these differences. The final accuracies of the XCTD temperatures and salinities were estimated to be the same as that of the CTD. During the two legs of the cruise, a total of 189 CTD and 120 XCTD profiles were obtained (Figure 2). The distance between stations is typically 7.5 km in the boundary current region and 12.5 km in the interior.

Shipboard acoustic Doppler current profiler (ADCP) data were collected throughout the cruise from *Alliance's* 75 kHz Ocean Surveyor transducer using the manufacturer's VMDAS collection software (Teledyne RDInstruments). A GPS/internal navigation-aided heading device (POSMV) provided high quality ship's heading as well as position information. The data were processed onboard in near-real time using the University of Hawaii's CODAS software package. The processing included bottom track calibrations, which compared ADCP-measured ship's movement relative to the sea floor with the GPS-derived ship's track in order to confirm the ADCP's alignment. Additional manual edits were applied to remove aliased velocity measurements due to elevated sea state, including forward bias where, under poor conditions, the measured ADCP velocity relative to the transducer can drift toward zero. Combined with the ship velocity, this produces an error in the direction of the ship's motion. Note that while the measurement depth of 75 kHz ADCP reached 600 m, most of the ADCP velocities below 300 m were removed during the quality control and manual editing processes. Barotropic tides were estimated using the Oregon State University's OTIS model (http://www.tpxo.net/regional, Iceland 1/60° model, described in Våge et al., 2013) and removed from the ADCP velocity data.

Vertical sections of potential temperature, salinity, and thermal wind relative to the sea surface were constructed with a vertical resolution of 10 m and a horizontal resolution of 5 km, using Laplacian-spline interpolation (Pickart & Smethie, 1998). The gridded thermal wind sections were then made absolute by using the same gridded sections of cross-track shipboard ADCP velocity as reference. For each pair of grid points in the thermal wind and the shipboard ADCP velocity sections, the referencing was done over the depth range 50–250 m, resulting in sections of absolute geostrophic velocity. The uncertainty of the shipboard ADCP velocity is taken to be approximately 3 cm/s (Våge et al., 2011). The volume transport error is

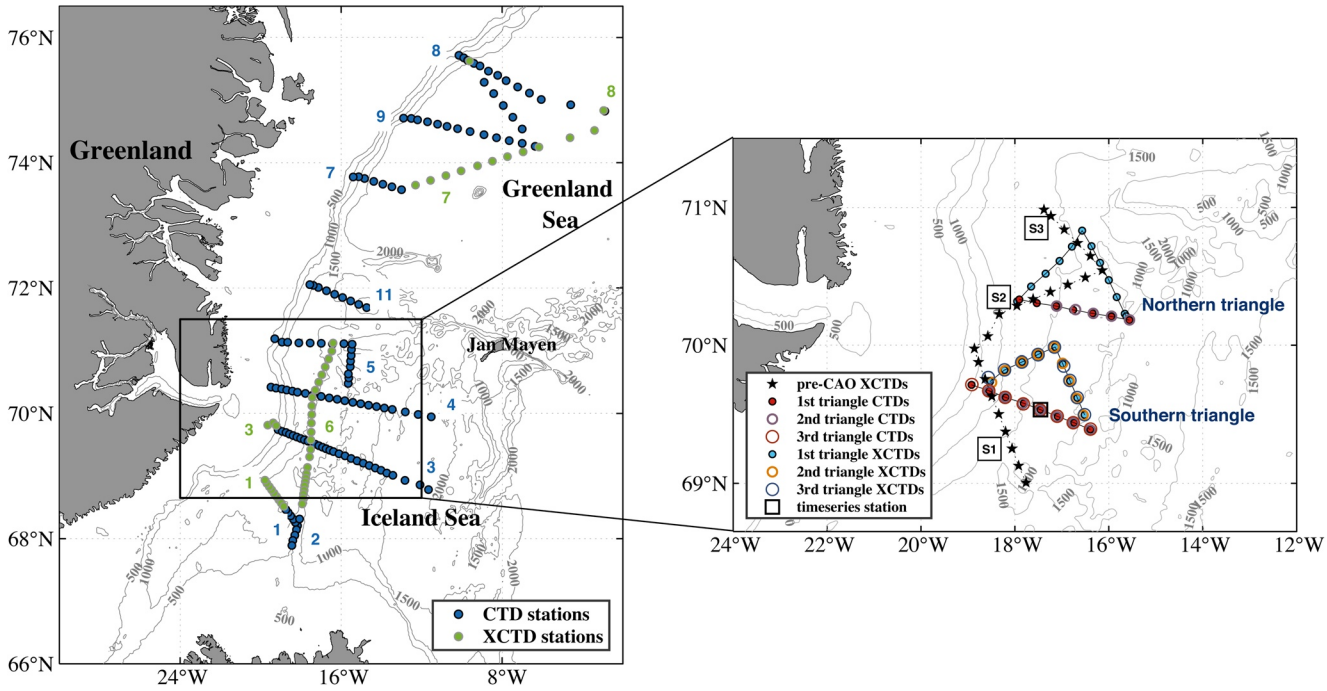

Figure 2. (left) Stations comprising the hydrographic sections occupied during the Iceland-Greenland Seas Project (IGP) winter cruise. The section numbers are listed. The box delimits the region shown in the right-hand panel. (right) Stations comprising the local hydrographic surveys carried out in the western Iceland Sea. The two triangle surveys were repeated several times. The type of instrument used for the sections and surveys are shown in the legend of the two panels. The bathymetry (gray contours) is from ETOPO2.

proportional to the area of current, e.g., the transport error is 0.3 Sv for a current with a width of 20 km over the upper 500 m.

2.2. Summer Cruise Data

To investigate seasonal differences of the water masses and velocity in the boundary current region, we use data from a summer cruise conducted by the RRS *James Clark Ross* (JCR) in July-August 2012. Four of the summertime transects were occupied within the IGP domain (see Figure 3). A similar setup of a Sea-Bird 911+ CTD mounted on a frame with twelve 10-L Niskin bottles was used to collect the hydrographic data. Velocity profiles were obtained at each station using a lowered ADCP. The same procedures were used to create gridded sections of hydrographic variables, thermal wind, lowered ADCP velocity and absolute geostrophic velocity. A detailed description of these summer cruise data is presented by Håvik, Pickart, et al. (2017).

2.3. One-Dimentional Mixing Model

The Price-Weller-Pinkel (PWP) mixed layer model (Price et al., 1986) was used to investigate wintertime water mass transformation under different forcing scenarios. The model has been used successfully in previous studies to simulate changes of mixed layer properties in the western Nordic Seas (Moore et al., 2015; Våge et al., 2018). The model was forced using heat flux and wind stress over a range of values, dictated by the winter (January to March) ERA5 reanalysis data from 2008 to 2018 provided by the European Center for Medium-Range Weather Forecasts (https://www.ecmwf.int/en/forecasts/datasets/reanalysis-datasets/era5).

2.4. Ekman Transport

The onshore Ekman transport displacement (x) was estimated by

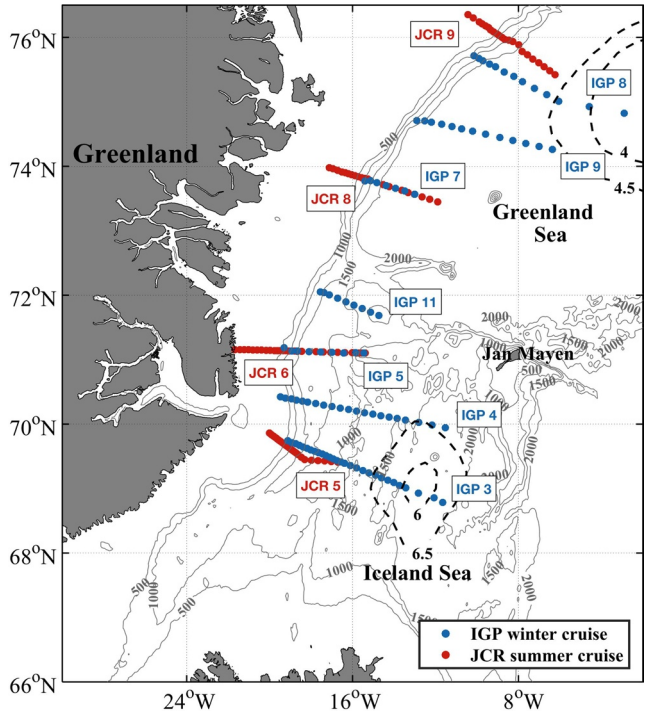

Figure 3. Locations of the sections across the East Greenland Current (EGC), occupied during the Iceland-Greenland Seas Project (IGP) winter cruise (blue) and James Clark Ross (JCR) summer cruise (red). The names of sections are noted. The climatological locations of the Iceland and Greenland Sea gyres are denoted by the dashed black lines, which are contours of surface dynamic height (dyn-cm) relative to 500 dbar, from Huang et al. (2020).

$$x = \int \frac{1}{\rho f h}\left[\tau_y(t) - \tau_y(t_0)\right] dt \quad (1)$$

where $\tau_y(t)$ is timeseries of the along-coast component of wind stress obtained from the ERA5 reanalysis (dt = 3 hours), t_0 is the initial time, ρ = 1027 kg/m^3 is the reference density of sea water, f is the Coriolis parameter, and h is the thickness of the Ekman layer.

3. Results

3.1. Wintertime Products in the Western Iceland and Greenland Seas

3.1.1. Water Masses and Their Distributions

Rather than adopt previously defined water mass definitions, which contain subjective criteria (e.g., the choice of a particular isotherm to distinguish between water types), we base our analysis on three unique end-members (Figure 4): the cold and fresh Polar Surface Water (PSW); the warm and relatively saline AtOW; and the cold and dense ArOW. Following Mastropole et al. (2017), for each water parcel we then computed the percentage contribution from the three end-members (PSW = −1.42 ± 0.18°C and 34.07 ± 0.11; AtOW = 2.50 ± 0.66°C and 34.98 ± 0.05; and ArOW = −0.63 ± 0.08°C and 34.92 ± 0.01, indicated in Figure 4a). These end members are the same as those used in Mastropole et al. (2017) (defined using an historical data set, see Figure 6 of Mastropole et al., 2017 for a geographical context), and the results presented below are not sensitive to the precise choices. Figure 4b shows the percentage contribution of each end member to the IGP data points from Figure 4a, where percentages >55% are colored (otherwise the data points are gray). Only

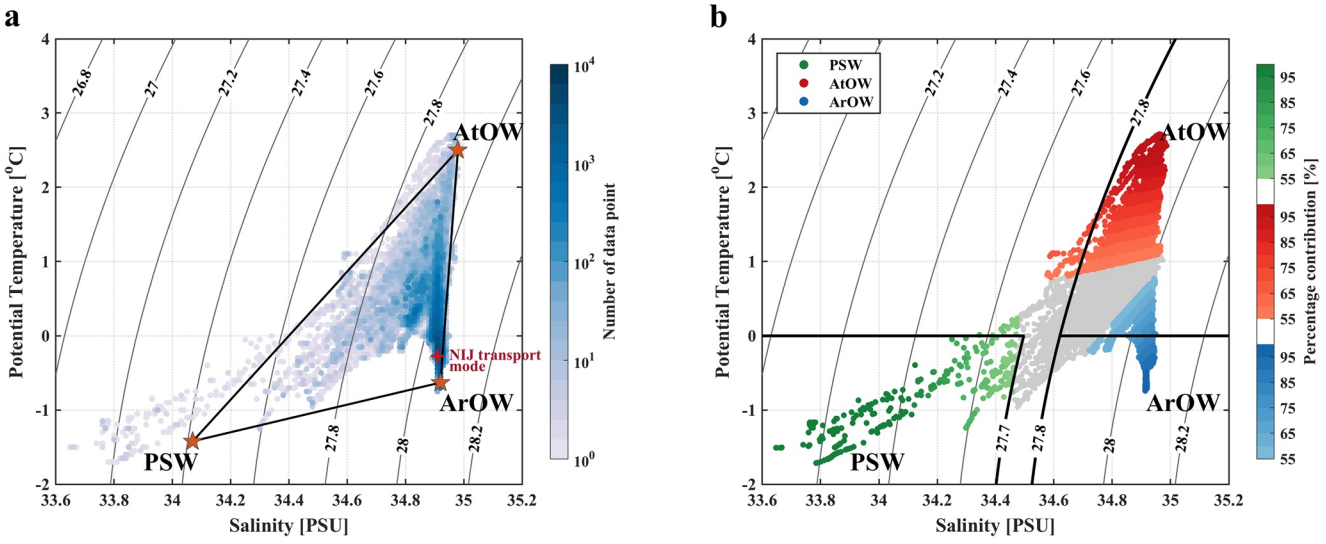

Figure 4. Potential temperature/salinity diagram for all the stations occupied during the Iceland-Greenland Seas Project (IGP) winter cruise. The color in (a) denotes the number of points within bins of 0.05°C in temperature by 0.01 in salinity. The three end-member water masses are marked by red stars. Polar Surface Water (PSW): −1.42 ± 0.18°C, 34.07 ± 0.11; Atlantic-origin Overflow Water (AtOW): 2.50 ± 0.66°C, 34.98 ± 0.05; and Arctic-origin Overflow Water (ArOW): −0.63 ± 0.08°C, 34.92 ± 0.01. The North Icelandic Jet (NIJ) transport mode is indicated by the red cross. The color in (b) denotes the percentage contributions of the three end-member water masses. The water mass boundaries defined in previous studies (e.g., Håvik, Pickart, et al. 2017; Våge et al., 2011) are outlined by the thick black lines in (b).

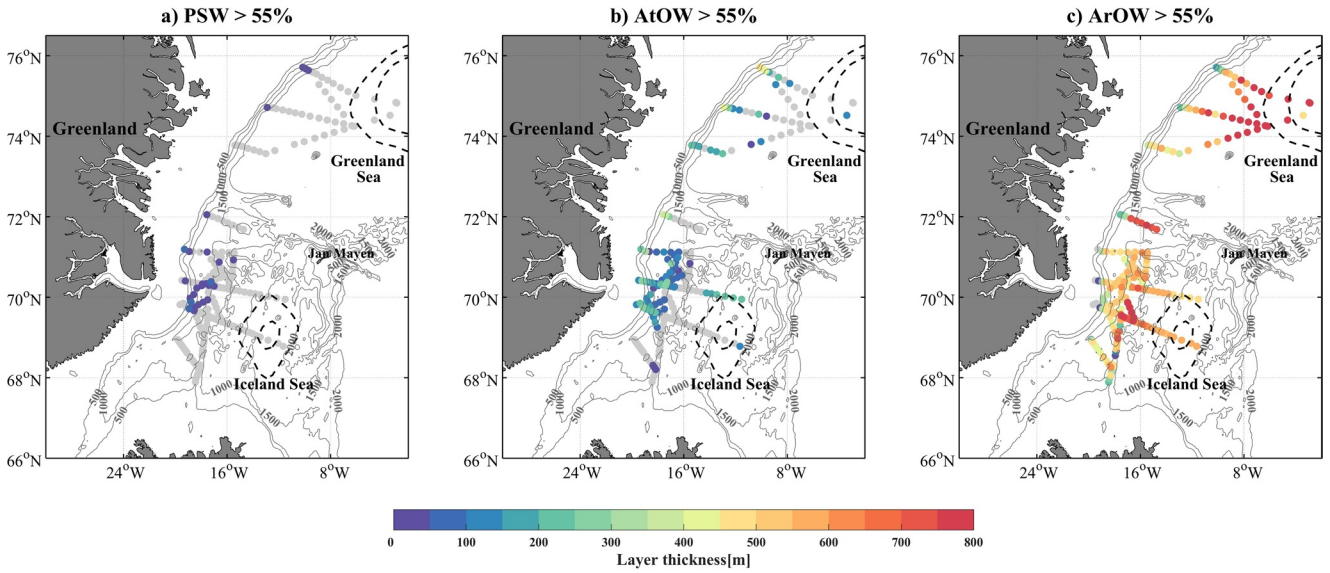

Figure 5. Spatial distribution of (a) Polar Surface Water (PSW), (b) Atlantic-origin Overflow Water (AtOW), and (c) Arctic-origin Overflow Water (ArOW) with the layer thickness in the upper 800 m of water column indicated by the color. Gray circles denote the profiles where these water masses were not found.

a small number of water parcels fall outside the mixing triangle (Figure 4a), and the slightly >100% contributions were forced to be 100%.

Here we assume that a given water parcel corresponds to one of the three water masses when it has more than 55% contribution from the corresponding end member. In general, the PSW so defined is consistent with that used in previous studies ($\sigma_\theta \leq 27.7$ kg/m^3 and $\theta < 0$°C: Rudels et al., 2002 and Håvik, Pickart, et al., 2017). The major difference between our classification system and those employed by earlier studies pertains to the boundary of AtOW and ArOW. In particular, some of dense water with temperatures greater than zero (0–0.7°C) is identified as ArOW in this study. In light of the recent warming of dense overflow water (e.g., Huang et al., 2020; Pickart et al., 2017), this makes sense.

During the IGP winter cruise, only a small amount of PSW was observed relative to the AtOW and ArOW (compare the number of data points in Figure 4). Figure 5a shows the spatial distribution of layer thickness of the PSW measured at each station. In the western Greenland Sea, only a small amount of PSW (layer thickness <100 m) was found on the upper continental slope. Farther south, more PSW was found offshore of the slope in the western Iceland Sea (with no significant change in the layer thickness). This regional difference in PSW presence is not surprising considering the enhanced instability of EGC in the Iceland Sea, which leads to a greater flux of properties from the slope to the interior (Håvik et al., 2019; Våge et al., 2013). Previous studies suggested that the distribution of PSW plays an important role in influencing the formation of deep mixed layers in the western Iceland and Greenland Seas (Våge et al., 2018). Details of how this water impacts wintertime water mass transformation in the vicinity of boundary current and in the interior are presented below in Sections 3.3.2 and 3.4.1, respectively. The distribution of AtOW in the western Iceland and Greenland Seas is generally similar to the PSW (Figure 5b), except that occurrences of AtOW were found farther into the interior, including within the Iceland and Greenland Sea gyres. The layer thickness of AtOW ranges from 0 to 450 m, with the maximum thickness found in the western boundary of the northern-most section. The densest water mass, ArOW, was observed in most of the stations in the western Iceland and Greenland Seas (Figure 5c). The layer thickness of this water mass decreased from the interior to the boundary current region, with a mean value of 470 ± 200 m (standard deviation).

3.1.2. Hydrographic Structure

Vertical sections of potential temperature and salinity were constructed for each of the transects occupied during the IGP winter cruise. Here we select two wintertime sections to show the typical hydrographic

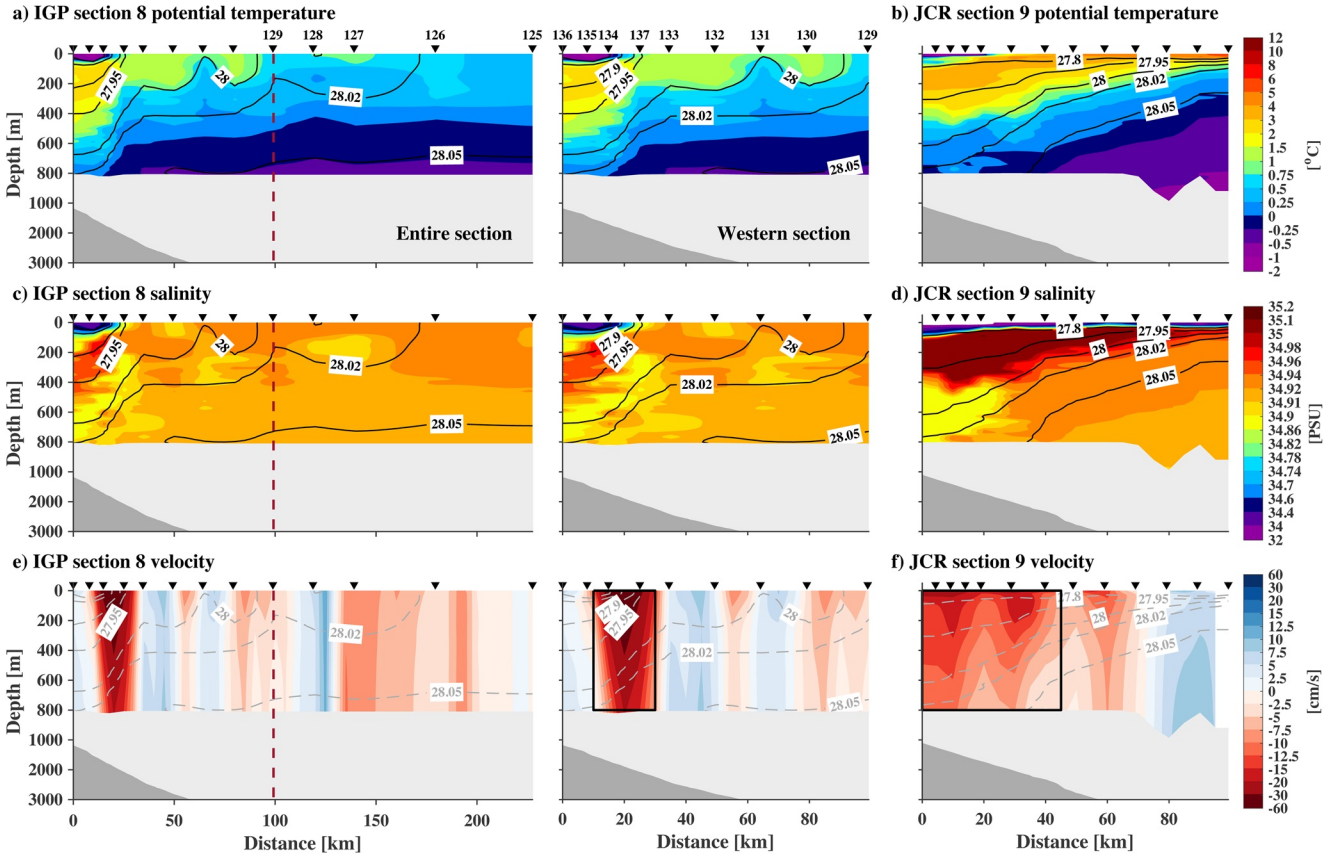

Figure 6. Vertical sections of (a), (b) potential temperature, (c), (d) salinity, and (e), (f) absolute geostrophic velocity, overlain by contours of potential density (kg/m^3), for Iceland-Greenland Seas Project (IGP) section 8 (the entire section on the left and the western portion (west of the dashed line) on the right) and James Clark Ross (JCR) section 9 in the western Greenland Sea. The locations of two sections are shown in Figure 3. The stations are marked by the black inverted triangles. The thick black boxes in (e) and (f) indicate the locations of East Greenland Current (EGC) in those two sections (see text). The bathymetry is from the ship's echosounder.

structure in the western Greenland and Iceland Seas. The first section (IGP section 8) extends across the continental slope of east Greenland into the western side of the Greenland Sea gyre (the location of the section is shown in Figure 3). The strongly sloped isopycnals on the western side of the section (Figure 6a) are associated with the EGC. While the CTD casts extended only to 800 m depth in this section, the three-layered hydrographic structure of EGC is evident: cold and fresh PSW near the surface, warm and saline AtOW located below, and cold and dense ArOW in the deep layer (see Figures 6a and 8a). Immediately offshore of the PSW, the AtOW was in direct contact with the atmosphere and hence was being ventilated. Further seaward, some of the deep isopycnals (e.g., 28.00 and 28.02 kg/m^3) outcrop, meaning that ventilation of ArOW was also taking place as well, in the transition region between the boundary current and gyre. We note that the spatial distribution of isopycnal outcropping was highly variable during the 43-days IGP cruise.

The second section (IGP section 3, see Figure 3 for location) extends across the boundary current in the Iceland Sea far enough into the interior to cross most of the gyre. Based on our criterion, there was no PSW present (as the highest percentage of PSW was less than 55%). The AtOW (stations 34–37) was being ventilated within the boundary current (see Figures 7a and 8c). In the open ocean region (>150 km), the Iceland Sea gyre is characterized by generally cold and fresh water at the surface. As with IGP section 8, outcropping isopycnals were observed in the transition region (from 50 to 100 km) between the boundary current and gyre. However, the isopycnals in question were less dense (27.95–27.97 kg/m^3) than farther north in the western Greenland Sea. When this section was reoccupied later in the cruise, PSW was present and extended well offshore. This variable distribution of PSW is likely associated with the instability of the EGC and/or the variable wind forcing this time of year.

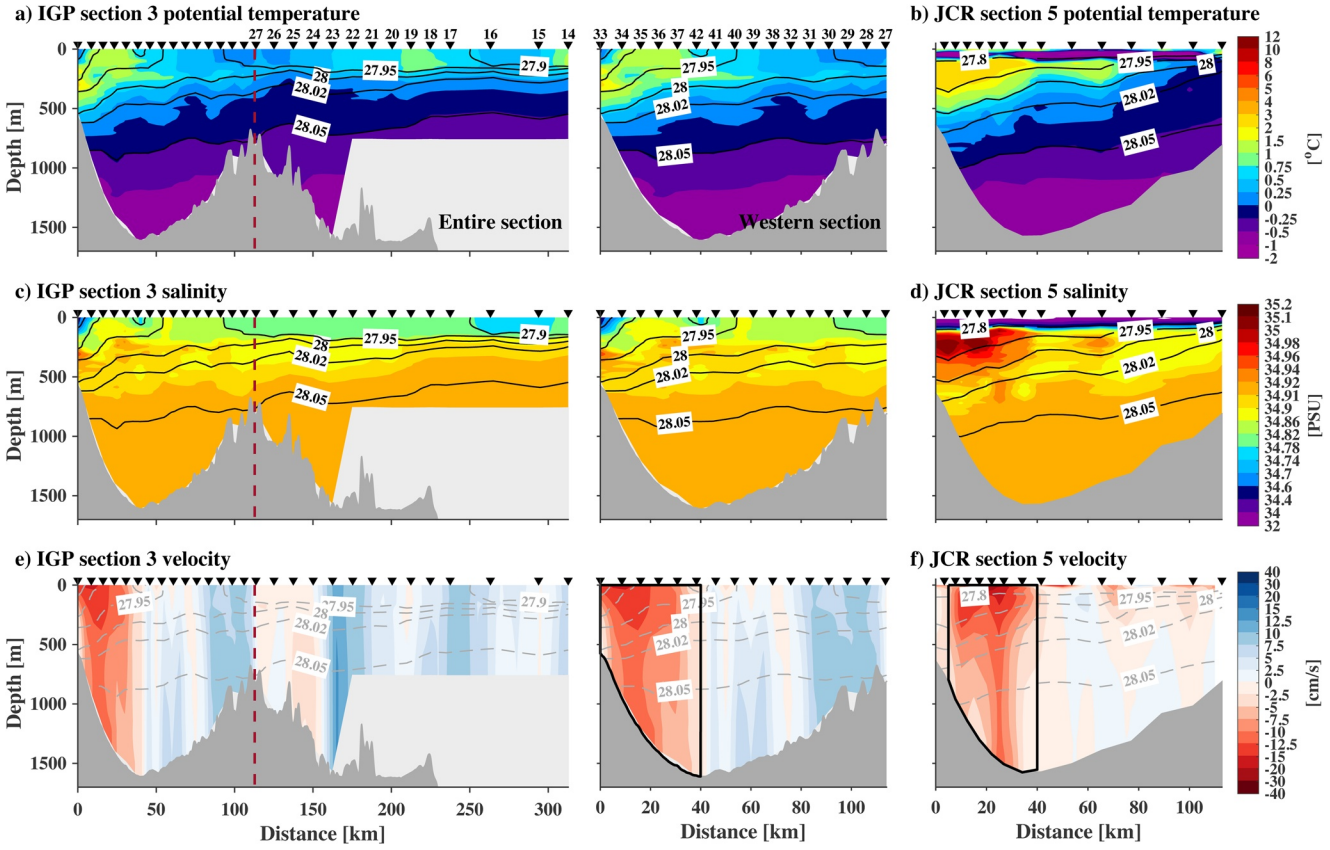

Figure 7. Vertical sections of hydrography and absolute geostrophic velocity for Iceland-Greenland Seas Project (IGP) section 3 and James Clark Ross (JCR) section 5 in the western Iceland Sea (see Figure 6 caption for details).

To investigate seasonal differences of the hydrographic structure in the EGC region, we use the summertime data from the JCR cruise. However, we first need to demonstrate that the differences in these two datasets do not reflect the fact that they were collected in different years. To accomplish this, we used the historical hydrographic data set from Huang et al. (2020) to construct a mean winter and summer vertical profile of temperature and salinity in the vicinity of the EGC. We used all profiles within 50 km of the 650 m isobath, for which there were 392 stations in summer and 92 in winter. We then did the same using the IGP hydrographic data (68 winter profiles) and JCR hydrographic data (88 summer profiles). This revealed that the differences in temperature and salinity between the IGP-averaged vertical profiles and JCR-averaged vertical profiles were comparable to the differences between the climatological winter and summer profiles.

We now compare two summertime sections from the JCR cruise (JCR sections 9 and 5) that were approximately aligned with two wintertime IGP sections (IGP section 8 and 3, see Figure 3). During both winter and summer, the warm and saline Atlantic water was present in the upper 600 m, and the isopycnals of the EGC sloped consistently upward offshore (see Figures 6a–6d, 7a–d, and 8). However, there are several notable seasonal differences in the hydrographic sections. First, the fresh PSW extended eastward and occupied the entire surface layer during the summer period (Figures 6d, 7d, 8b and 8d). Second, the slope of the isopycnals (e.g., 27.9 and 27.95 kg/m^3 isopycnals) was weaker during the summer period. These differences are robust in the climatological fields (e.g., Våge et al., 2018) and are reasonable in light of the seasonality of the wind forcing in the western Iceland and Greenland Seas. Woodgate et al. (1999) noted that the strongly sloped isopycnals in winter are indicative of onshore Ekman transport driven by the strong northerly wind. Våge et al. (2018) demonstrated that the wind-induced onshore Ekman transport in fall/early winter is sufficient to push much of the PSW toward the shelfbreak. Interestingly, the isopycnal slope in the deep layer (e.g., the 28.02 and 28.05 kg/m^3 isopycnals) was greater in summer than in winter, opposite to the change in the upper layer. This difference can be explained by the seasonal export of dense overflow water from the

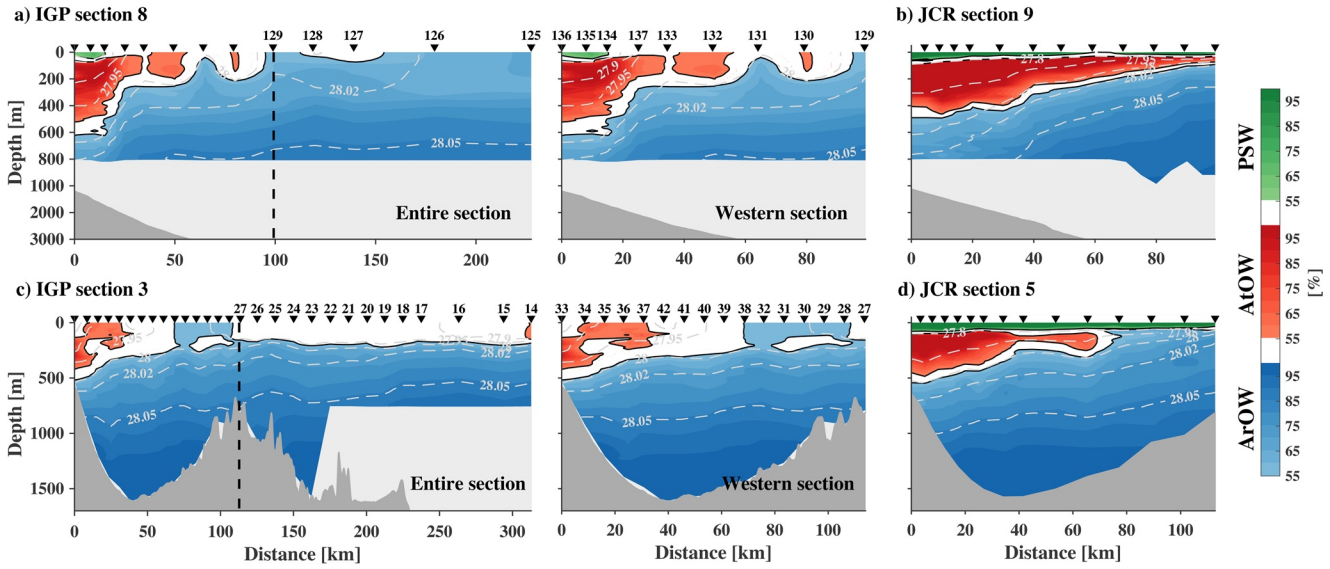

Figure 8. Vertical sections of the percentage contributions (color) of the end-member water masses. (a) Iceland-Greenland Seas Project (IGP) section 8; (b) James Clark Ross (JCR) section 9; (c) IGP section 3; (d) JCR section 5. The contours of 55% contribution and potential density are denoted by the solid black lines and the gray dashed lines, respectively.

interior of the Greenland and Iceland Seas under the impact of wind stress curl (Huang et al., 2020; Yang & Pratt, 2012).

In addition to the vertical hydrographic structure, we document the wintertime mixed-layer properties. In general, the mixed layers in the Iceland and Greenland Seas are densest and deepest in late winter (February to April) due to the seasonal ventilation under strong atmospheric forcing (Brakstad et al., 2019; Våge et al., 2015). By analyzing the late-winter mixed layer properties in the Iceland Sea, Våge et al. (2015) hypothesized that part of the ArOW in the NIJ originates from the northwest Iceland Sea outside of the gyre. However, there are only sparse historical data in this region to support this hypothesis.

The mixed layer characteristics (temperature, salinity, density, and depth) for the roughly 300 hydrographic profiles collected in February and March 2018 were determined by performing a multi-step procedure applied to the density, temperature, and salinity profiles (Brakstad et al., 2019; Pickart et al., 2002; Våge et al., 2015). During the IGP cruise, the deepest (>300 m) and densest (>28.03 kg/m^3) mixed layers were found in the western Greenland Sea (Figure 9), although the mixed layer depths in this region were highly variable. In addition, the northwestern Iceland Sea also stands out as a region of somewhat deep (150–200 m) and dense (27.92–27.98 kg/m^3) mixed layers, though to a lesser extent than the Greenland Sea. Our results imply that the mixed layers in the western Iceland Sea were not sufficiently dense to supply the densest component of ArOW during this year, but that ventilation of this component was occurring in the Greenland Sea. This is consistent with the results of Huang et al. (2020), who analyzed all available hydrographic data from the Nordic Seas over the period 1986–2015. We note, however, that the NAO was in a positive phase and the atmospheric forcing was weak during the first part of the IGP cruise, which would result in weak convection. During the previous winters the regional air-sea fluxes were stronger (e.g., Renfrew et al., 2019) and the mixed layers were deeper and denser (e.g., Brakstad et al., 2019; Våge et al., 2015). To further investigate the source of ArOW, the PWP model is used to assess mixed layer properties in the interior under strong atmospheric forcing, which is presented in Section 3.4.2.

3.2. Velocity Structure in the Western Iceland and Greenland Seas

A broad-scale view of the circulation in the western Iceland and Greenland Seas during the wintertime IGP cruise is presented in Figure 10, which shows a map of the depth-averaged (50–250 m) shipboard ADCP velocity. The strongest velocities in each section were found along the continental slope, associated with the EGC. Seaward of the slope, velocities were generally weaker and highly variable. There was no clear

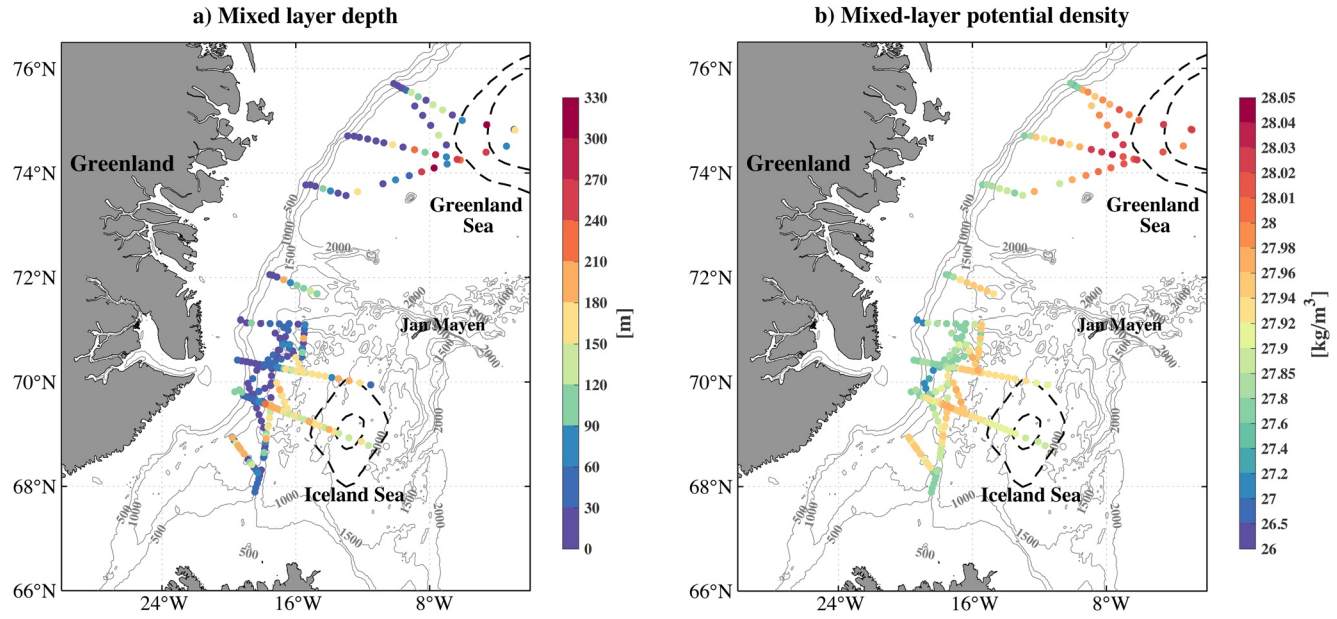

Figure 9. (a) Mixed layer depth [m] and (b) mixed layer potential density [kg/m^3] for the Iceland-Greenland Seas Project (IGP) winter cruise.

evidence of the gyre circulation in either basin. Part of the variability in the interior is due to the presence of eddies, which were frequently encountered throughout the cruise.

Vertical sections of absolute geostrophic velocity were constructed by referencing the thermal wind to the directly measured velocity (see Methods Section). Here we show two wintertime and two summertime velocity sections (Figures 6e, 6f, 7e and 7f) corresponding to the previously presented hydrographic sections. One sees that the surface-intensified EGC was prominent on the western side of the sections during both time periods, associated with strongly sloped isopycnals. The vertical shear in velocity of the EGC was stronger (due to the stronger sloped isopycnals) in winter than in summer (e.g., Figures 6e and 6f, from 10 to 30 km). This is consistent with the seasonal change in the kinematic structure of the EGC observed from moorings north of Denmark Strait (Håvik, Våge, et al., 2017). Furthermore, we find that the width of the EGC was narrower and the velocity in the core of EGC was stronger in the northern IGP section versus the southern one (compare Figures 6e and 7e). Such a relationship between EGC width and strength was also found during the summertime JCR survey (Håvik, Pickart, et al., 2017). Håvik, Pickart, et al. (2017) identified two distinct components of the EGC in JCR section (Figure 6f): the shelfbreak EGC (from 0 to 45 km), and what they referred to as the outer EGC (from 50 to 65 km). The latter feature was linked to the recirculation of the West Spitsbergen Current in Fram Strait. However, we only observed the shelfbreak EGC in the wintertime section (Figure 6e). Offshore of this, anticyclonically rotating features were associated with patches of AtOW (Figures 6a and 8a). Details of the impact of these eddies on the wintertime water mass transformation in the interior are presented in Section 3.4.1.

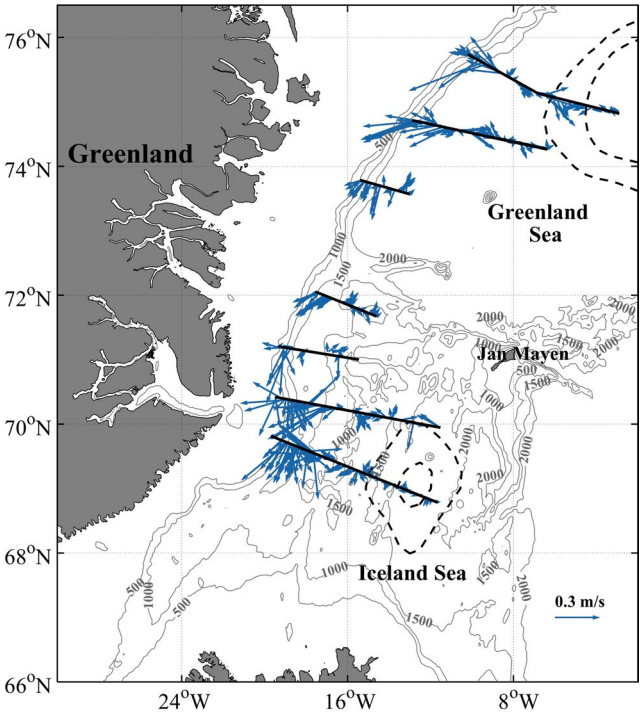

Figure 10. Depth-averaged (50–250 m) velocity vectors for the seven sections across the East Greenland Current (EGC) during the Iceland-Greenland Seas Project (IGP) winter cruise.

Using the hydrographic and velocity vertical sections, we calculated the volume transport of PSW, AtOW and ArOW (the water with >55% contribution from the respective end-member water mass) in the EGC. Here we focus on the AtOW, which is transported to Denmark Strait primarily via the EGC. Following Håvik, Pickart, et al. (2017), the left and right bounding limits of the EGC were chosen as the locations where the depth-mean

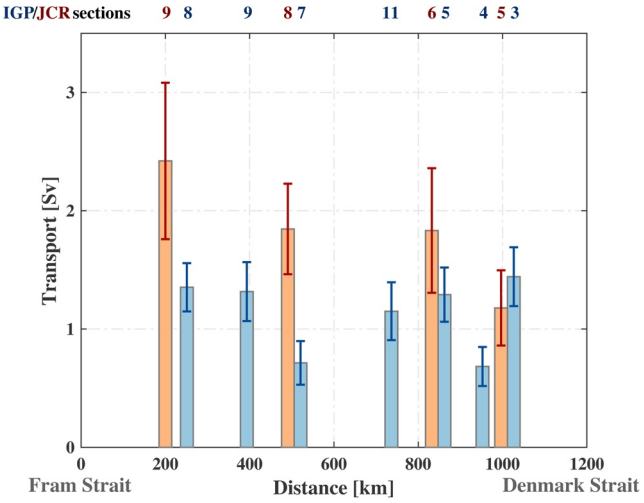

Figure 11. Volume transport of Atlantic-origin Overflow Water (AtOW) in the East Greenland Current (EGC) for each of the sections of the Iceland-Greenland Seas Project (IGP) winter cruise (blue bars) and James Clark Ross (JCR) summer cruise (orange bars). The *x* axis indicates the along-stream distance from Fram Strait to Denmark Strait. The uncertainty is the measurement error.

velocity over the upper 150 m was reduced to 20% of the core value (indicated by the black boxes in the velocity sections of Figures 6e and 6f and 7e and 7f). For the seven sections occupied during the IGP winter cruise, the mean volume transport of AtOW in the EGC is 1.1 ± 0.1 Sv (the uncertainty is the standard deviation). This transport is smaller than the mean transport of 1.8 ± 0.2 Sv from the four sections occupied during the JCR summer cruise. While Håvik, Pickart, et al. (2017) found that the volume transport of AtOW decreased from north to south along the pathway of the EGC in summer, there was no such a trend found during the IGP winter cruise (Figure 11). The variability in the volume transport of AtOW was mainly dictated by the water mass constituents in the EGC, rather than the velocity structure. We note that the AtOW estimates above are based on our definition of AtOW. For the AtOW defined previously by the choice of the 0°C isotherm (see Figure 4b), the mean volume transport for the IGP winter cruise is 3.2 ± 0.7 Sv, which is slightly larger than that for the JCR summer cruise, 2.8 ± 0.7 Sv.

3.3. Water Mass Transformation in the Western Iceland and Greenland Seas: Vicinity of the Boundary Current

3.3.1. Along-Stream Water Mass Transformation

While previous cruises have investigated water mass transformation in the EGC from Fram Strait to Denmark Strait as part of a single survey, none of them were occupied in winter. Here we present details of wintertime water mass transformation along the pathway of the EGC and compare it with the summertime JCR result. We extracted the profiles within the EGC for the IGP winter cruise and JCR summer cruise, where the criteria for defining the bounding limits of the EGC are described above in Section 3.2. For each section, we used the profiles within the EGC to compute a single averaged profile (at each depth layer the mean temperature and salinity were obtained by averaging the values at the same depth layer), and these are presented in the θ/S plane in Figure 12a. Two seasonal differences are notable. First, there was only a small amount of PSW in the upper

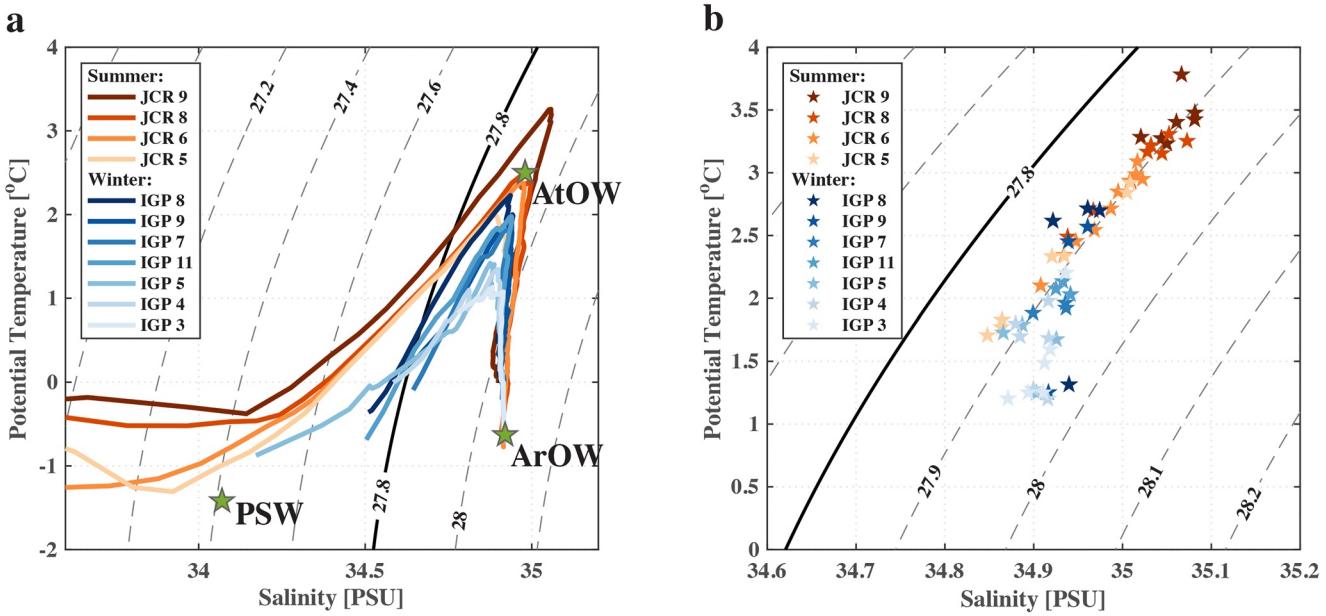

Figure 12. Potential temperature/salinity diagram for (a) the mean profiles, and (b) the core of the Atlantic-origin Overflow Water (AtOW) (the intermediate temperature maximum layer) in the East Greenland Current (EGC) for each of the Iceland-Greenland Seas Project (IGP) sections. The sections are indicated by different colors (see the legend). The end-member water masses are marked by the green stars in (a).

layer of the water column during the winter period (see also Figures 6–8). Second, the warmest portion of the AtOW is colder (by 1°C) and less saline (by 0.01) in winter than in summer. Furthermore, AtOW generally becomes colder and less saline from the northern to the southern sections during both the summer and winter periods (Figure 12a). This implies that transformation of this water mass along the pathway of EGC occurs throughout the year.

To investigate how AtOW is transformed in the EGC, we focus on the along-stream change in the hydrographic properties of the core of this water mass. Following Håvik, Pickart, et al. (2017), the core of AtOW was identified by the intermediate temperature maximum for each CTD profile inside the EGC. The properties of AtOW for the EGC stations at the different sections are marked by different colored symbols in Figure 12b. During the summer, the properties of the core are gradually modified approximately along the 27.9 kg/m^3 isopycnal from north to south, indicating that isopycnal mixing is the main mechanism. In contrast, the properties of the AtOW in the EGC were also modified diapycnally during the winter, mostly via a change in temperature. This change mainly occurred for the seaward-most stations in the EGC, which is addressed in the next section.

3.3.2. Water Column Response to a Cold-Air Outbreak

As discussed in the Introduction, most of the wintertime air-sea heat exchange in the Iceland and Greenland Seas occurs during cold air outbreaks. These typically last 2–4 days and occur every 1–2 weeks (Harden et al., 2015). During the IGP winter cruise, several weather products from the Icelandic Met Office, the UK Met Office, and the Danish Meteorological Institute, were sent daily to the ship. Based on a forecast of a cold-air outbreak (CAO) in the western Iceland Sea beginning on 1 March, the ship steamed to the region and commenced a sampling pattern to measure the oceanographic response. This included repeating a short section several times over the course of the CAO (the base of the southern triangle in Figure 2b) and occupying a timeseries station (also marked in Figure 2b). While the CAO was long-lived (lasting more than 10 days), it was not a particularly cold event (the temperature of the cold air mass over the region was slightly above the long-term winter mean for the period of 1979–2018, see Renfrew et al., 2019). Nonetheless, the atmospheric forcing over the region intensified during the first part of the event. In particular, the northerly wind increased from 8–10 to 15–20 m/s, and the net air-sea total heat flux increased from 150 to 200 to more than 300 W/m^2 (Figures 13a and 13d, where positive values indicate heat loss from the ocean). We now compare a composite hydrographic section occupied prior to the increase in heat flux (pre-CAO sampling, on March 1–2) to a section occupied when the atmospheric forcing had moderated (after-CAO sampling, on March 6). The location of the section is shown in Figures 13a and 13d. We note that the ship was unable to readily sample in the marginal ice zone; this could only be done in good conditions during daylight hours. As such, the repeat section extended only onshore enough to capture the offshore edge of the EGC. The timeseries CTD station (station T5 in Figure 13) was occupied on March 1, 2, 3, 6, and 10.

There were significant changes in the water column at the offshore edge of the boundary current between the pre-CAO and after-CAO hydrographic sections (Figures 13b, 13c, 13e and 13f). In particular, the PSW cap at the surface was displaced onshore during the event, and strong vertical mixing was evident at station T3 (see Figures 13b, 13c, 13e and 13f). The mixed layer density at station T3 increased from 27.8 kg/m^3 to 27.9 kg/m^3. What led to these changes? Våge et al. (2018) and Spall et al. (2021) suggested that strong northerly winds in winter can divert the surface fresh water onto the Greenland shelf via enhanced onshore Ekman transport. To examine this, we estimated the onshore Ekman transport displacement (Equation 1 in Section 2.4) over the time period between the occupation of the two sections. Assuming a surface Ekman layer of 60 m (the surface freshwater layer, see Figures 13b and 13c), the displacement is 10–15 km. This estimate is consistent with the observed onshore displacement of the freshwater front (compare Figures 13b, 13c, 13e and 13f). Note that a comparable thickness of the Ekman layer (50 m) was also assumed by Våge et al. (2018), and this choice is in line with that estimated based on the similarity height (defined as μ_*/f, where μ_* is the friction velocity and f is the Coriolis parameter, see Mofjeld & Lavelle, 1984). In addition to advection, the displacement of the front was influenced by vertical mixing. The deepened and densified mixed layer at station T3 is the result of the slightly warmer and saltier seaward edge of PSW being cooled and mixed downwards due to the atmospheric forcing. Note that any further such mixing would penetrate the warm, salty Atlantic water layer.

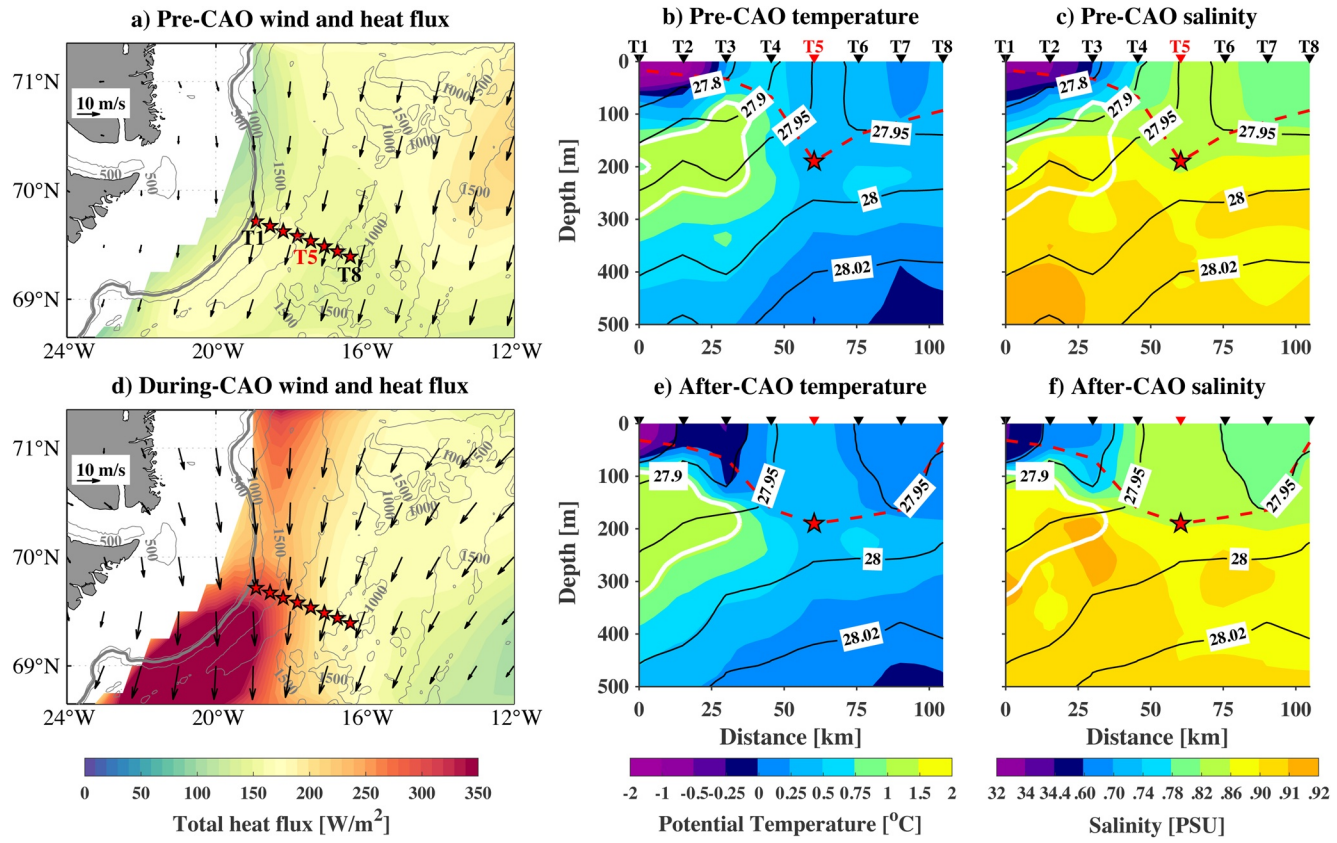

Figure 13. (a) Pre-cold-air outbreak (Pre-CAO) (March 1–2) and (d) During-CAO (March 5) 10-m wind (vectors) and total heat flux (color). The location of the repeated hydrographic section is shown by the red stars, and the timeseries station T5 is labeled. (b)–(c) Pre-CAO and (e)–(f) After-CAO (March 6) vertical sections of potential temperature and salinity (color), overlain by contours of potential density (kg/m^3). The conductivity-temperature-depth (CTD) stations are marked by the black inverted triangles except for station T5 that is marked in red. The depth of mixed layer at each station is denoted by the red dashed line, with station T5 marked by the red star. The contours of 55% contribution of the Atlantic-origin Overflow Water (AtOW) end member are indicated by the white lines.

Farther offshore, at station T5, the mixed layer was slightly warmer and saltier after the CAO, despite the high heat loss to the atmosphere. This was the location of the timeseries station, which indicated that the mixed layer became continually warmer and saltier through the entire event (not shown). Where did the heat come from? We suspect that it was provided via lateral mixing from the core of AtOW in the EGC. Note that at station T5, the depth of mixed layer (the red star in Figure 13b) reaches the depth of the core of the AtOW (indicated by the white contours in Figures 13b and 13e) within the EGC. A lateral transfer of heat from warm AtOW (below the Ekman layer) could compensate the heat loss due to the air-sea interaction. Our results thus imply that ventilation of AtOW can take place via convection at the offshore edge of the EGC, while, seaward of this, lateral turbulent flux from the core of AtOW can moderate the water mass transformation.

3.4. Water Mass Transformation in the Western Iceland and Greenland Seas: Interior

We now investigate the water mass transformation in the interior of western Iceland and Greenland Seas, and how this is influenced by mesoscale variability.

3.4.1. Eddy Activity

During nearly every section occupied on the cruise we encountered isolated patches of AtOW seaward of the EGC. On four of the sections these corresponded to well-defined anticyclonic eddies (we assume that the other patches were also associated with eddies but were not resolved properly). Here we show two vertical sections that nicely captured anticyclonic eddies. The first example is from IGP section 4 in the

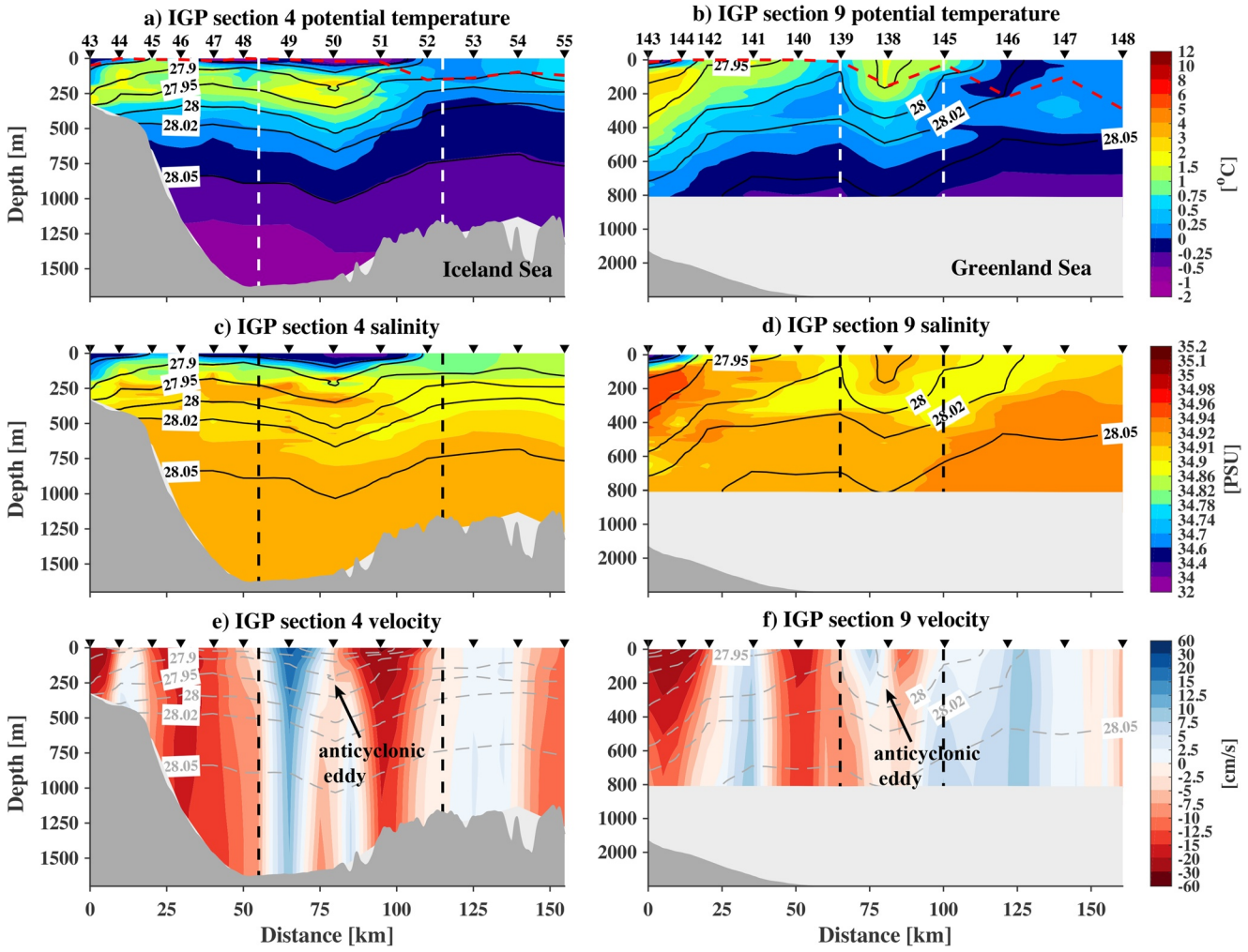

Figure 14. Vertical sections of (a), (b) potential temperature, (c), (d) salinity, and (e), (f) absolute geostrophic velocity, overlain by contours of potential density (kg/m^3), for Iceland-Greenland Seas Project (IGP) sections 4 and 9. The locations of the anticyclonic eddies are delimited by the vertical dashed lines. The mixed layer depth at each station is denoted by the red dashed line in (a) and (b).

western Iceland Sea (Figures 14a, 14c and 14e). The eddy had a diameter of approximately 60 km, and was associated with a pronounced downward vertical deflection of the isopycnals and strong anticyclonic rotation (roughly 30 cm/s). The same three-layered hydrographic structure as that in the EGC was found in the eddy, which indicates that the feature originated from the boundary current. As shown in Spall et al. (2008), an unstable shelfbreak current spawns dipole pairs which self-propagate into the interior, after which the cyclonic partner spins down more rapidly than the anticyclonic partner. The eddies formed here brought a large amount of PSW into the interior (see Figures 14a and 14c). The presence of the freshwater prohibited convection (the mean mixed layer inside the eddy was about 100 m shallower than the stations on the eastern side of the eddy, Figure 14a). We note that this eddy was observed at very beginning of cruise and still resided at nearly the same location one month later during the occupation of a north-south XCTD line (Figure 2a; which also confirms that this was an isolated eddy and not a meander of the EGC). This implies that such a strong eddy could prohibit convection for much of the winter (keeping in mind that 2018 was a weaker winter than normal, see Section 3.4.2 for details).

A second example of an anticyclone is from IGP section 9 (about 450 km north of section 4) in the western Greenland Sea (Figures 14b, 14d and 14f). Compared with the feature to the south, this eddy was smaller in diameter (approximately 30 km) with weaker rotation speed (about 10 cm/s). Notably, there is no evidence of freshwater at the surface of this anticyclonic eddy. Instead, it was comprised of warm and saline AtOW

in the surface layer. We suspect that this eddy had a weaker PSW signature when formed, which was eroded due to air-sea buoyancy loss and convection. In contrast with the southern feature, the mixed layer in this eddy was deeper than the surrounding stations (by about 50–100 m, Figure 14b), and contained newly ventilated AtOW. These two examples demonstrate that eddies shed from the EGC can play differing roles in modifying/prohibiting open ocean convection.

Håvik, Pickart, et al. (2017) observed numerous eddy features during the summer JCR cruise but the majority of them were cyclones. It is unclear why the cyclonic partner would be longer lived in the summer; it could be that there is seasonality in the evolution of these features as they progress offshore. This and other questions regarding the nature of these eddies require further study. Unfortunately, we are unable to use either multi-satellite mapped or along-track sea surface products in this region to track eddies because of the large uncertainty of altimetric signals due to the sea ice cover (the two eddies shown above were not detectable in the altimeter field). Previous studies have suggested that wind-induced vertical processes (e.g., vertical mixing) are active in the periphery of eddies (Gaube et al., 2015; McGillicuddy et al., 2007). Further investigation is also required to determine how these eddy-wind interactions might impact the wintertime transformation of overflow water.

3.4.2. Assessing Mixed Layer Development Using a 1-D Mixing Model

The mixed layer properties presented above in Section 3.1.2 suggest that the ArOW mainly sources from the Greenland Sea, rather than the northwestern Iceland Sea (consistent with the results of Huang et al., 2020 using historical data). While we did not observe extensive ventilation of this water mass during the cruise, recall that winter 2018 was anomalously weak. Compared with the climatological mean from 1979 to 2018, the mean 2-m air temperature in the region was more than one standard deviation warmer, the mean wind speed was slightly weaker, and the mean turbulent heat loss was roughly 30 W/m^2 less during the time period of the IGP cruise (see Figure 10 in Renfrew et al., 2019). To explore what the mixed layer products might have been under stronger atmospheric forcing, we used the PWP model. In particular, we used the profiles collected during the IGP cruise as initial conditions, and forced them with large heat loss and strong surface wind stress. Since the PWP model is one-dimensional, lateral processes such as advection are not included; as such, we considered only stations outside of the EGC. We note that the model was successfully used to reproduce the evolution of the mixed-layer depth and properties at stations seaward of the EGC during the CAO by forcing the model with the realistic wind stress and air-sea heat flux from ERA5. This provides confidence in our results below.

According to the ERA5 reanalysis in recent years (2008–2018), the wintertime (January to March) monthly total heat loss and wind stress in the western Iceland and Greenland Seas are in the ranges 50–200 W/m^2 and 0.05–0.3 N/m^2, respectively. To maximize the effect of strong atmospheric forcing, we forced the PWP model with a constant value of 200 W/m^2 and a southward windstress of 0.3 N/m^2, and ran the simulation for two months (CTD casts with a freshwater cap were excluded from the calculation since these formed ice). This is meant to account for the fact that preconditioning of the water column was weak prior to the cruise (the NAO was in a positive phase in December and January), and that convection would normally continue into early April (Våge et al., 2015). Comparison of the mixed layer properties before and after the two-month simulation is presented in the θ/S plane in Figure 15. The properties of the NIJ transport mode of ArOW (the water with the highest transport within the NIJ and also the densest component of ArOW, $\overline{\sigma_\theta} = 28.05$ kg/m^3, Semper et al., 2019) are indicated by the intersection of the black dashed lines. Under the impact of strong atmospheric forcing, the mixed layer depths become deeper for all profiles, with the deepest layers (>500 m) still occurring in the western Greenland Sea (note that some of the CTD casts only extended to 800 m). In both seas there is significant cooling of the mixed layers after two months of strong forcing. Notably, some of the mixed layer properties in the western Greenland Sea closely match those of the NIJ transport mode, in contrast to the mixed layers in the western Iceland Sea which are fresher and less dense. This suggests that ventilation of the NIJ transport mode could occur on the periphery of the Greenland Sea gyre if the forcing is strong enough, in addition to the center of the gyre (Huang et al., 2020).

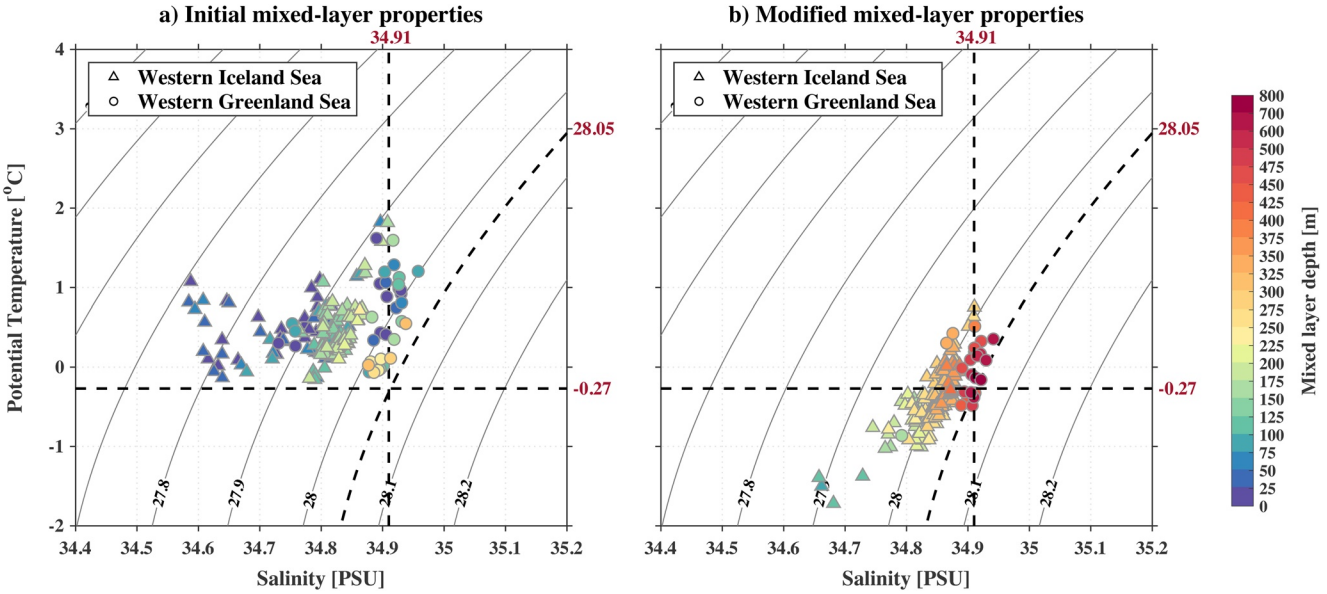

Figure 15. (a) Initial and (b) Price-Weller-Pinkel-modified mixed layer properties based on the Iceland-Greenland Seas Project (IGP) winter cruise data. The properties in the western Iceland Sea and Greenland Sea are shown by triangles and circles, respectively. The color indicates the depth of the mixed layer. The properties (density, temperature and salinity) of the North Icelandic Jet (NIJ) transport mode of Arctic-origin Overflow Water (ArOW) are indicated by the intersection of the black dashed lines.

4. Summary

Data from a 2018 winter survey of the western Iceland and Greenland Seas were analyzed to better understand the ventilation of dense overflow water feeding Denmark Strait. The characteristics and distribution of wintertime water masses and aspects of the circulation were described and compared with results from a previous summer survey. It was found that the Atlantic-origin Overflow Water (AtOW) mainly resided in the vicinity of the East Greenland Current (EGC). Progressing from north to south, the properties of AtOW in the EGC were modified diapycnally during the winter, in contrast to along-isopycnal transformation of this water in the summer. Direct ventilation of AtOW in winter was observed on the offshore side of the EGC. A 10-days cold-air outbreak occurred in early March during which the Polar Surface Water (PSW) cap at the surface of the EGC was displaced onshore, and strong vertical mixing took place at the seaward edge of EGC due to the enhanced northerly wind and air-sea heat flux. Just offshore of this, lateral transfer of heat and salt from the core of AtOW in the EGC appears to have compensated the heat loss from air-sea interaction, modifying the water mass transformation.

Arctic-origin Overflow Water (ArOW) was mainly found in the interior of Iceland and Greenland Seas. The observed mixed layers containing this water mass were not dense enough to ventilate the transport mode of the North Icelandic Jet (NIJ), although the atmospheric forcing was generally weak during winter 2018. To investigate the evolution of the mixed layers under stronger atmospheric forcing, we used the PWP 1-D mixing model. This demonstrated that some of the ArOW product in the interior of western Greenland Sea matched that of the NIJ transport mode when subject to such air-sea forcing, while in the western Iceland Sea the mixed layers were fresher and less dense than the transport mode. This is consistent with previous results suggesting that the northwest Iceland Sea only supplies a small fraction of the densest ArOW (Huang et al., 2020; Våge et al., 2015).

During the IGP winter cruise a number of anticyclonic eddies spawned from the EGC were observed in the interior. We highlighted two such features: one in the Iceland Sea and one in the Greenland Sea. The eddy in the Iceland Sea eddy was strong and contained a pronounced cap of PSW that prohibited convection. By contrast, the Greenland Sea eddy was relatively weak with no evidence of a freshwater cap at the surface. Instead, AtOW was being ventilated within the feature. This implies that eddies shed from the boundary current play differing roles in modifying/prohibiting open-ocean convection in the interior of the western

Iceland and Greenland Seas. Further investigation is required to quantify the bulk impact of eddies on the wintertime transformation of overflow water in the western Nordic Seas.

Data Availability Statement

The final hydrographic and shipboard velocity data for the IGP and JCR cruises are available at https://web.whoi.edu/all0118/and kogur.whoi.edu/php/index.php.

Acknowledgments
The authors thank the crew members and scientists of the NRV *Alliance* for collecting the IGP cruise data. We thank L. Håvik for providing the processed summer cruise data. Funding was provided by the National Science Foundation under grant OCE-1558742.

References

Behrens, E., Våge, K., Harden, B., Biastoch, A., & Böning, C. W. (2017). Composition and variability of the Denmark Strait Overflow Water in a high-resolution numerical model hindcast simulation. *Journal of Geophysical Research: Oceans*, *122*(4), 2830–2846. https://doi.org/10.1002/2016jc012158

Brakstad, A., Våge, K., Håvik, L., & Moore, G. W. K. (2019). Water mass transformation in the Greenland Sea during the period 1986–2016. *Journal of Physical Oceanography*, *49*(1), 121–140. https://doi.org/10.1175/jpo-d-17-0273.1

Chafik, L., & Rossby, T. (2019). Volume, heat, and freshwater divergences in the subpolar North Atlantic suggest the Nordic Seas as key to the state of the meridional overturning circulation. *Geophysical Research Letters*, *46*, 4799–4808. https://doi.org/10.1029/2019gl082110

deJong, M. F., Søiland, H., Bower, A. S., & Furey, H. H. (2018). The subsurface circulation of the Iceland Sea observed with RAFOS floats. *Deep Sea Research Part I: Oceanographic Research Papers*, *141*, 1–10. https://doi.org/10.1016/j.dsr.2018.07.008

deSteur, L., Hansen, E., Gerdes, R., Karcher, M., Fahrbach, E., & Holfort, J. (2009). Freshwater fluxes in the East Greenland Current: A decade of observations. *Geophysical Research Letters*, *36*(23). https://doi.org/10.1029/2009gl041278

deSteur, L., Hansen, E., Mauritzen, C., Beszczynska-Möller, A., & Fahrbach, E. (2014). Impact of recirculation on the East Greenland Current in Fram Strait: Results from moored current meter measurements between 1997 and 2009. *Deep Sea Research Part I: Oceanographic Research Papers*, *92*, 26–40. https://doi.org/10.1016/j.dsr.2014.05.018

Dickson, R. R., & Brown, J. (1994). The production of North Atlantic Deep Water: Sources, rates, and pathways. *Journal of Geophysical Research*, *99*(C6), 12319–12341. https://doi.org/10.1029/94jc00530

Eldevik, T., Nilsen, J. E. Ø., Iovino, D., Olsson, K. A., Sandø, A. B., & Drange, H. (2009). Observed sources and variability of Nordic seas overflow. *Nature Geoscience*, *2*(6), 406–410. https://doi.org/10.1038/ngeo518

Fahrbach, E., Meincke, J., Østerhus, S., Rohardt, G., Schauer, U., Tverberg, V., & Verduin, J. (2001). Direct measurements of volume transports through Fram Strait. *Polar Research*, *20*(2), 217–224. https://doi.org/10.1111/j.1751-8369.2001.tb00059.x

Foldvik, A., Aagaard, K., & Tørresen, T. (1988). On the velocity field of the East Greenland Current. *Deep Sea Research Part I: Oceanographic Research Papers*, *35*(8), 1335–1354. https://doi.org/10.1016/0198-0149(88)90086-6

Gaube, P., Chelton, D. B., Samelson, R. M., Schlax, M. G., & O'Neill, L. W. (2015). Satellite observations of mesoscale eddy-induced Ekman pumping. *Journal of Physical Oceanography*, *45*(1), 104–132. https://doi.org/10.1175/jpo-d-14-0032.1

Hansen, B., & Østerhus, S. (2000). North Atlantic–Nordic Seas exchanges. *Progress in Oceanography*, *45*(2), 109–208. https://doi.org/10.1016/s0079-6611(99)00052-x

Harden, B., Pickart, R. S., Valdimarsson, H., Våge, K., de Steur, L., Richards, C., et al. (2016). Upstream sources of the Denmark Strait Overflow: Observations from a high-resolution mooring array. *Deep Sea Research Part I: Oceanographic Research Papers*, *112*, 94–112. https://doi.org/10.1016/j.dsr.2016.02.007

Harden, B., Renfrew, I., & Petersen, G. (2015). Meteorological buoy observations from the central Iceland Sea. *Journal of Geophysical Research: Atmospheres*, *120*(8), 3199–3208. https://doi.org/10.1002/2014jd022584

Håvik, L., Almansi, M., Våge, K., & Haine, T. W. N. (2019). Atlantic-origin Overflow Water in the East Greenland Current. *Journal of Physical Oceanography*, *49*(9), 2255–2269. https://doi.org/10.1175/jpo-d-18-0216.1

Håvik, L., Pickart, R. S., Våge, K., Torres, D. J., Thurnherr, A. M., Beszczynska-Möller, A., et al. (2017). Evolution of the East Greenland Current from Fram Strait to Denmark Strait: Synoptic measurements from summer 2012. *Journal of Geophysical Research: Oceans*, *122*(3), 1974–1994. https://doi.org/10.1002/2016jc012228

Håvik, L., & Våge, K. (2018). Wind-driven coastal upwelling and downwelling in the shelfbreak East Greenland Current. *Journal of Geophysical Research: Oceans*, *123*(9), 6106–6115. https://doi.org/10.1029/2018jc014273

Håvik, L., Våge, K., Pickart, R. S., Harden, B., von Appen, W. J., Jónsson, S., & Østerhus, S. (2017). Structure and variability of the shelfbreak East Greenland Current north of Denmark Strait. *Journal of Physical Oceanography*, *47*(10), 2631–2646. https://doi.org/10.1175/jpo-d-17-0062.1

Huang, J., Pickart, R. S., Huang, R. X., Lin, P., Brakstad, A., & Xu, F. (2020). Sources and upstream pathways of the densest overflow water in the Nordic Seas. *Nature Communications*, *11*, 5389. https://doi.org/10.1038/s41467-020-19050-y

Jahnke-Bornemann, A., & Brümmer, B. (2008). The Iceland—Lofotes pressure difference: Different states of the North Atlantic low-pressure zone. *Tellus A: Dynamic Meteorology and Oceanography*, *61*(4), 466–475. https://doi.org/10.1111/j.1600-0870.2009.00401.x

Jonsson, S., & Valdimarsson, H. (2004). A new path for the Denmark Strait overflow water from the Iceland Sea to Denmark Strait. *Geophysical Research Letters*, *31*, L03305. https://doi.org/10.1029/2003gl019214

Käse, R. H., Serra, N., Köhl, A., & Stammer, D. (2009). Mechanisms for the variability of dense water pathways in the Nordic Seas. *Journal of Geophysical Research*, *114*(C1), C01013. https://doi.org/10.1029/2008jc004916

Köhl, A. (2010). Variable source regions of Denmark Strait and Faroe Bank Channel overflow waters. *Tellus A: Dynamic Meteorology and Oceanography*, *62*(4), 551–568. https://doi.org/10.1111/j.1600-0870.2010.00454.x

Köhl, A., Käse, R. H., Stammer, D., & Serra, N. (2007). Causes of changes in the Denmark Strait overflow. *Journal of Physical Oceanography*, *37*(6), 1678–1696. https://doi.org/10.1175/jpo3080.1

Lin, P., Pickart, R. S., Jochumsen, K., Moore, G. W. K., Valdimarsson, H., Fristedt, T., & Pratt, L. (2020). Kinematic structure and dynamics of the Denmark Strait overflow from ship-based observations. *Journal of Physical Oceanography*, *50*(11), 3235–3251. https://doi.org/10.1175/jpo-d-20-0095.1

Mastropole, D., Pickart, R. S., Valdimarsson, H., Våge, K., Jochumsen, K., & Girton, J. (2017). On the hydrography of Denmark Strait. *Journal of Geophysical Research: Oceans*, *122*(1), 306–321. https://doi.org/10.1002/2016jc012007

Mauritzen, C. (1996). Production of dense overflow waters feeding the North Atlantic across the Greenland-Scotland Ridge. Part 1: Evidence for a revised circulation scheme. *Deep Sea Research Part I: Oceanographic Research Papers*, *43*(6), 769–806. https://doi.org/10.1016/0967-0637(96)00037-4

McGillicuddy, D. J., Anderson, L. A., Bates, N., Bibby, T., Buesseler, K. O., Carlson, C. A., et al. (2007). Eddy/wind interactions stimulate extraordinary mid-ocean plankton blooms. *Science*, *316*(5827), 1021–1026. https://doi.org/10.1126/science.1136256

Mofjeld, H. O., & Lavelle, J. W. (1984). Setting the length scale in a second-order closure model of the unstratified bottom boundary layer. *Journal of Physical Oceanography*, *14*, 833–839. https://doi.org/10.1175/1520-0485(1984)014<0833:stlsia>2.0.co;2

Moore, G. W. K., Renfrew, I. A., & Pickart, R. S. (2012). Spatial distribution of air-sea heat fluxes over the sub-polar North Atlantic. *Geophysical Research Letters*, *39*, L18806. https://doi.org/10.1029/2012gl053097

Moore, G. W. K., Våge, K., Pickart, R. S., & Renfrew, I. A. (2015). Decreasing intensity of open-ocean convection in the Greenland and Iceland seas. *Nature Climate Change*, *5*(9), 877–882. https://doi.org/10.1038/nclimate2688

Nilsson, J., Björk, G., Rudels, B., Winsor, P., & Torres, D. J. (2008). Liquid freshwater transport and Polar Surface Water characteristics in the East Greenland Current during the AO-02 Oden expedition. *Progress in Oceanography*, *78*(1), 45–57. https://doi.org/10.1016/j.pocean.2007.06.002

Olsen, S. M., Hansen, B., Quadfasel, D., & Østerhus, S. (2008). Observed and modeled stability of overflow across the Greenland–Scotland ridge. *Nature*, *455*(7212), 519–522. https://doi.org/10.1038/nature07302

Pickart, R. S., & Smethie, W. M., Jr (1998). Temporal evolution of the deep western boundary current where it enters the sub-tropical domain. *Deep Sea Research Part I: Oceanographic Research Papers*, *45*(7), 1053–1083. https://doi.org/10.1016/s0967-0637(97)00084-8

Pickart, R. S., Spall, M. A., Torres, D. J., Våge, K., Valdimarsson, H., Nobre, C., et al. (2017). The North Icelandic Jet and its relationship to the North Icelandic Irminger Current. *Journal of Marine Research*, *75*(5), 605–639. https://doi.org/10.1357/002224017822109505

Pickart, R. S., Torres, D. J., & Clarke, R. A. (2002). Hydrography of the Labrador Sea during active convection. *Journal of Physical Oceanography*, *32*(2), 428–457. https://doi.org/10.1175/1520-0485(2002)032<0428:hotlsd>2.0.co;2

Price, J. F., Weller, R. A., & Pinkel, R. (1986). Diurnal cycling: Observations and models of the upper ocean response to diurnal heating, cooling, and wind mixing. *Journal of Geophysical Researc*, *91*(C7), 8411–8427. https://doi.org/10.1029/jc091ic07p08411

Renfrew, I. A., Pickart, R. S., Våge, K., Moore, G. W. K., Bracegirdle, T. J., Elvidge, A. D., et al. (2019). The Iceland Greenland seas project. *Bulletin of the American Meteorological Society*, *100*(9), 1795–1817.

Rudels, B., Björk, G., Nilsson, J., Winsor, P., Lake, I., & Nohr, C. (2005). The interaction between waters from the Arctic Ocean and the Nordic Seas north of Fram Strait and along the East Greenland Current: Results from the Arctic Ocean-02 Oden expedition. *Journal of Marine Systems*, *55*(1–2), 1–30. https://doi.org/10.1016/j.jmarsys.2004.06.008

Rudels, B., Fahrbach, E., Meincke, J., Budéus, G., & Eriksson, P. (2002). The East Greenland Current and its contribution to the Denmark Strait overflow. *ICES Journal of Marine Science*, *59*(6), 1133–1154. https://doi.org/10.1006/jmsc.2002.1284

Semper, S., Våge, K., Pickart, R. S., Valdimarsson, H., Torres, D. J., & Jónsson, S. (2019). The emergence of the North Icelandic Jet and its evolution from northeast Iceland to Denmark Strait. *Journal of Physical Oceanography*, *49*(10), 2499–2521. https://doi.org/10.1175/jpo-d-19-0088.1

Spall, M. A., Almansi, M., Huang, J., Haine, T. W. N., & Pickart, R. S. (2021). Lateral redistribution of heat and salt in the Nordic Seas. *Progress in Oceanography*, *196*, 102609. https://doi.org/10.1016/j.pocean.2021.102609

Spall, M. A., Pickart, R. S., Fratantoni, P. S., & Plueddemann, A. J. (2008). Western Arctic Shelfbreak Eddies: Formation and transport. *Journal of Physical Oceanography*, *38*, 1644–1668. https://doi.org/10.1175/2007jpo3829.1

Swift, J. H., Aagaard, K., & Malmberg, S. A. (1980). The contribution of the Denmark Strait overflow to the deep North Atlantic. *Deep Sea Research*, *27A*, 29–42. https://doi.org/10.1016/0198-0149(80)90070-9

Våge, K., Moore, G. W. K., Jónsson, S., & Valdimarsson, H. (2015). Water mass transformation in the Iceland Sea. *Deep Sea Research Part I: Oceanographic Research Papers*, *101*, 98–109. https://doi.org/10.1016/j.dsr.2015.04.001

Våge, K., Papritz, L., Håvik, L., Spall, M. A., & Moore, G. W. K. (2018). Ocean convection linked to the recent ice edge retreat along east Greenland. *Nature Communications*, *9*(1), 1–8. https://doi.org/10.1038/s41467-018-03468-6

Våge, K., Pickart, R. S., Spall, M. A., Moore, G. W. K., Valdimarsson, H., Torres, D. J., et al. (2013). Revised circulation scheme north of the Denmark Strait. *Deep Sea Research Part I: Oceanographic Research Papers*, *79*, 20–39. https://doi.org/10.1016/j.dsr.2013.05.007

Våge, K., Pickart, R. S., Spall, M. A., Valdimarsson, H., Jónsson, S., Torres, D. J., et al. (2011). Significant role of the North Icelandic Jet in the formation of Denmark Strait overflow water. *Nature Geoscience*, *4*(10), 723–727. https://doi.org/10.1038/ngeo1234

Woodgate, R. A., Fahrbach, E., & Rohardt, G. (1999). Structure and transports of the East Greenland Current at 75 N from moored current meters. *Journal of Geophysical Research*, *104*(C8), 18059–18072. https://doi.org/10.1029/1999jc900146

Yang, J., & Pratt, L. J. (2012). On the effective capacity of the dense-water reservoir for the Nordic seas overflow: Some effects of topography and wind stress. *Journal of Physical Oceanography*, *43*, 418–431. https://doi.org/10.1175/JPO-D-12-087.1